Journal of Advanced Ceramics
2015, **4**(2): 103–110
DOI: 10.1007/s40145-015-0137-1

ISSN 2226-4108
CN 10-1154/TQ

Research Article

Fusion bonding and microstructure formation in TiB_2-based ceramic/metal composite materials fabricated by combustion synthesis under high gravity

Xuegang HUANG[a,*], Jie HUANG[a], Zhongmin ZHAO[b], Long ZHANG[b], Junyan WU[b]

[a]*Hypervelocity Aerodynamics Institute*, *China Aerodynamics Research and Development Center*, *Mianyang 621000*, *China*
[b]*Department of Vehicle and Electrical Engineering*, *Mechanical Engineering College*, *Shijiazhuang 050003*, *China*

Received: September 18, 2014; Revised: December 07, 2014; Accepted: December 09, 2014

Abstract: The novel ceramic/metal composite materials were successfully fabricated by combustion synthesis in high gravity field. In this paper, the Ti–B_4C was selected as the main combustion reaction system to obtain TiB_2–TiC ceramic substrate, and the 1Cr18Ni9Ti stainless steel was selected as the metal substrate. It was found that the TiB_2–TiC/1Cr18Ni9Ti composite materials exhibited continuously graded composition and hybrid microstructure. The TiC_{1-x} carbides and TiB_2 platelets decreased gradually in size and volume fraction from the ceramic to stainless steel. Due to the rapid action of thermal explosion as well as the dissolution of the molten stainless steel into TiB_2–TiC liquid, the diffusion-controlled concentration gradient from the ceramic liquid to the alloy liquid was observed. Finally, as a result of the rapid sequent solidification of the ceramic liquid and the melt alloy surface, the laminated composite materials were achieved in multilevel, scale-span hybrid microstructure.

Keywords: combustion synthesis; high gravity field; TiB_2–TiC/1Cr18Ni9Ti; hybrid microstructure

1 Introduction

Because of its high hardness, high corrosion resistance, good thermal shock resistance, and high temperature stability, TiB_2-based ceramic composites attract a lot of attention as the potential materials in engineering applications [1,2]. The novel TiB_2–TiC ceramic possesses more advantages than traditional metals, especially in high temperature techniques [3–5]. However, ceramics generally have low toughness and are hard to be used to manufacture complex parts. So it is necessary to manufacture these complex parts by joining ceramics and metals to meet the special requirements [6]. Over the past 50 years, various ceramic–metal joining techniques have been developed and improved, such as mechanical joining, adhesive joining, friction joining, high energy beam welding, microwave joining, ultrasonic welding, explosive welding, reaction joining, combustion reaction joining, field-assisted bonding, diffusion bonding, transient liquid phase bonding, partial transient liquid phase bonding, and so on [6]. However, most of these methods mentioned above need complicate equipment, extra energy supply, and long preparation time, which lead to the high production costs finally [7–9]. It is

* Corresponding author.
E-mail: emei-126@126.com

generally known that a key problem in joining ceramic and metal is the thermal expansion mismatch between them, which brings about high residual stress at the interface of the ceramic and the metal, thereby deteriorating mechanical properties of the ceramic–metal composite. Bever and Duwez [10] have pointed out that the functionally graded material (FGM) of the ceramic/metal can effectively mitigate the residual stress arising at ceramic–metal interface.

Combustion synthesis which was also called self-propagating high-temperature synthesis (SHS) is being used to produce ceramics, intermetallics, and composite materials [11–14]. Based on this technology, joining a ductile metal with a brittle ceramic composite matrix has considerable potential for substantial improvements in fracture toughness [15]. Recently, a rapid and economical processing named combustion synthesis in high gravity field has been applied to prepare bulk solidified TiB_2–TiC ceramics, and the high performance of TiB_2–TiC composites is presented due to the achievement in fine-grained and ultrafine-grained microstructures [5]. Subsequently, the laminated composite materials of TiB_2–TiC ceramic and Ti alloy in continuously graded microstructures were fabricated by employing combustion synthesis in high gravity field to accomplish fusion bonding of liquid ceramic to Ti alloy substrate [16]. Hence, based on the achievement in combustion synthesis in ultrahigh gravity field, another economical material of the laminated ceramic–steel composite develops. In the thesis, applying combustion synthesis in ultrahigh gravity field to achieve laminated composite materials of the ceramic on stainless steel substrate, and the microstructure and formation mechanism of the laminated composite of the ceramic on stainless steel are discussed.

2 Experimental

Commercial powders of Ti (99.5% purity, < 34 μm), B_4C (97% purity, < 3 μm), CrO_3 (99.9% purity, < 60 μm), and Al (96% purity, < 50 μm) were used as raw materials. The Ti to B_4C molar ratio of 3:1 was chosen as the starting composition based on Eq. (1), so the composition of the solidified TiB_2–TiC composite was determined as TiC:TiB_2 = 1:2. In order to ensure full-liquid products after the combustion reaction, the 30 wt% (CrO_3+Al) subsystem was added as the activator for increasing the combustion temperature according to Eq. (2).

$$3Ti + B_4C \rightarrow TiC + 2TiB_2 \quad (1)$$

$$CrO_3 + 2Al \rightarrow Al_2O_3 + Cr \quad (2)$$

The above powder blends were mechanically homogenized by ball milling for 1 h. The 1Cr18Ni9Ti stainless steel plate with thickness of 10 mm was placed at the bottom of the cylindrical graphite crucible, and then the crucible was filled with the mechanically activated raw blends (500 g) under uniaxially cold-press of about 200 MPa. After that, the prepared graphite crucible was fixed on the centrifugal machine. The combustion reaction was triggered with the electrically heated W wire (diameter of 0.5 mm), while the centrifugal machine provided a high gravity acceleration of 2000*g* (where *g* means the gravitational constant, $g = 9.8\ m/s^2$). When the combustion reaction was over, the centrifugal machine continued to run for 30 s. After the crucible was cooled to ambient temperature, the laminated composites of the ceramic and stainless steel were obtained.

The whole process of high gravity combustion synthesis and melt-infiltration can be described as the following three steps. First, the TiB_2–TiC ceramic melt and Al_2O_3 melt were obtained by the aluminothermic reactions in Eq. (1) and Eq. (2), respectively, and then the Al_2O_3 melt was separated from the ceramic due to the differences in density and wetting ability, and finally, TiB_2–TiC ceramic melt infiltrated into the fused surface of stainless steel substrate. After that, the Al_2O_3 oxide slag at the top of the sample should be removed by grinding. Figure 1 shows the cross-sectional image of TiB_2–TiC/1Cr18Ni9Ti composite materials without Al_2O_3 oxide slag. It also can be found that the surface of the stainless steel substrate is partially molten.

The phase composition was identified by X-ray diffraction (XRD; D/max-PA 2550PC, Rigaku, Japan) with a step of 0.02° and a scanning rate of 2 (°)/min. The microstructure and fracture morphology were

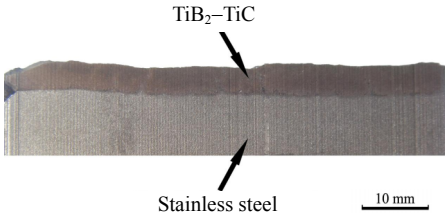

Fig. 1 Cross-sectional image of TiB_2–TiC/1Cr18Ni9Ti composite materials after the Al_2O_3 oxide slag has been removed.

examined by field emission scanning electron microscopy (FESEM; JSM-7001F, JEOL, Japan). Electron probe microanalysis (EPMA) was conducted by energy dispersive spectrometry (EDS).

3 Results and discussion

The results of XRD and FESEM show that the TiB_2–TiC ceramic is composed of fine TiB_2 platelets as the primary phase, irregular TiC grains as the secondary phase, and a few of Cr-based intermetallic binder as intercrystalline phase, as shown in Fig. 2 and Fig. 3. The density, hardness, and fracture toughness of the TiB_2–TiC ceramic are tested as 4.3 g/cm^3, 18±1.5 GPa, and 13.5±1.8 MPa·m$^{1/2}$, respectively. The combustion synthesis process in high gravity field for preparing TiB_2–TiC ceramic can be described as follows.

Based on Eq. (1) and Eq. (2), there are three liquid equilibrium products of TiC, TiB_2, Cr, and Al_2O_3 from combustion synthesis in terms of the thermodynamics of chemical reaction among the elements of Al, O, Ti, C, and B. According to the equilibrium diagram of the TiB_2–TiC system [1], the melting temperature of 66.7%TiB_2–TiC ceramic is around 2900 ℃, which is much smaller than the designed combustion temperature in current experiments, thus the full-liquid products of TiC, TiB_2, Cr, and Al_2O_3 can be achieved in combustion reaction. Because of the immiscibility and density difference between liquid TiB_2–TiC–Cr and Al_2O_3, the liquid-phase separation characterized by float-up of liquid Al_2O_3 and settle-down of liquid TiB_2–TiC–Cr rapidly takes place in high gravity field, resulting in the presence of the layered melt in the crucible. Finally, as the melt is cooled to ambient temperature, the layered sample is formed to present the solidified TiB_2–TiC ceramic with Cr metallic binder covered by the flux layer of Al_2O_3. At the same time, the surface of steel substrate is also melt due to the extremely high heat releasing of combustion reaction. FESEM images of Fig. 4 show that there is an irregular intermediate layer between the ceramic and the stainless steel, and a few randomly distributed Al_2O_3 inclusions are also observed in the region between the stainless steel substrate and the TiB_2–TiC ceramic, as shown by the arrows in Fig. 4. These isolated Al_2O_3 inclusions tend to distribute in the intermediate area near the stainless steel substrate. However, it is hard to find the Al_2O_3 inclusions in the intermediate area near the ceramic matrix. The above phenomenon derives from the good heat conductivity of the stainless steel, which results in the extremely high solidification rate of the TiB_2–TiC ceramic melt near the stainless steel substrate. Since some Al_2O_3 drops cannot be completely expelled out of the ceramic melt timely, these randomly distributed Al_2O_3 inclusions, then, remain in the intermediate layer.

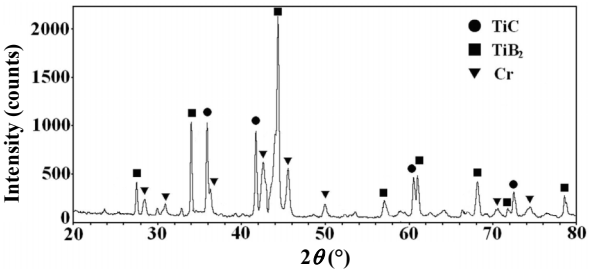

Fig. 2 XRD pattern of the TiB_2–TiC ceramic.

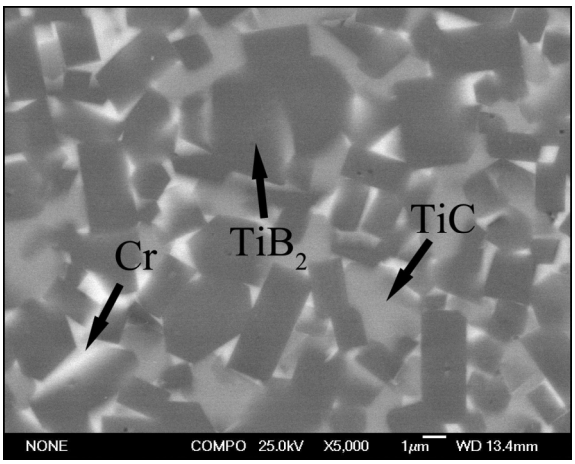

Fig. 3 FESEM microstructure of the TiB_2–TiC ceramic.

According to the results of FESEM and EDS in Fig. 5 and Table 1, it can be concluded that the intermediate layer within the network structure is mainly composed of TiB_2, TiC, Cr–Fe alloy, and solidified stainless steel. Meanwhile, with the distance increasing from the stainless steel substrate to the TiB_2-based ceramic, the volume fraction of Cr–Fe alloy phases drops sharply, whereas those of TiB_2 and TiC phases rise rapidly as shown by the EDS map scanning results of Fig. 6. So it can be inferred that with the increased distance in the intermediate from the stainless steel substrate, TiB_2 and TiC crystals become the main phases in the intermediate layer. Moreover, the ultrafine-grained microstructure of the

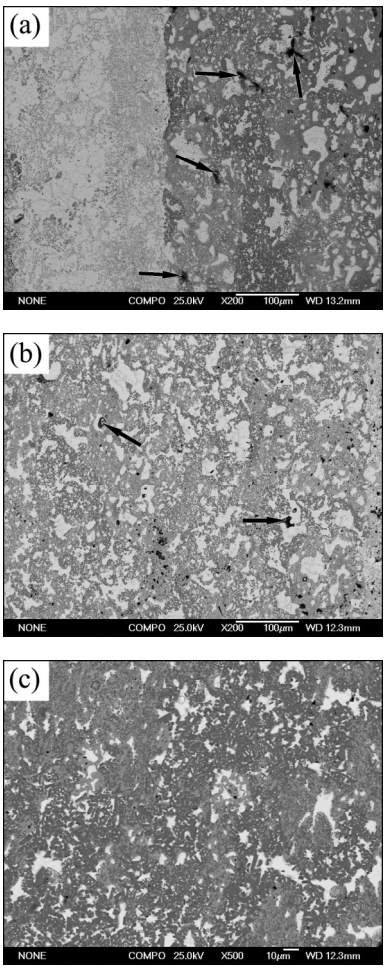

Fig. 4 FESEM images of the joint area of stainless steel and the ceramic: (a) interfacial area between solidified stainless steel and the intermediate layer; (b) the intermediate layer; (c) the intermediate area nearby the ceramic matrix.

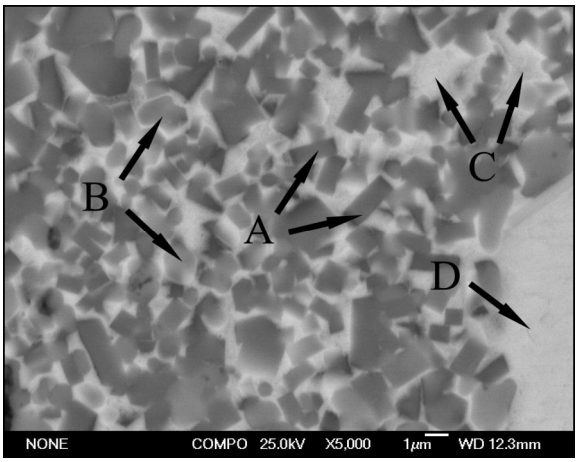

Fig. 5 FESEM image of ultrafine-grained microstructure at the intermediate area between the ceramic and the stainless steel.

Table 1 Composition of the intermediate layer between the ceramic and the stainless steel in Fig. 5 (unit: at%)

Position	Ti	C	B	Cr	Fe	Ni	Determined phase
A	31.88	—	62.91	1.08	1.16	2.97	TiB_2
B	47.02	42.79	—	4.46	2.46	3.27	TiC
C	13.01	—	—	57.10	27.11	2.78	Cr–Fe alloy
D	10.26	—	—	15.74	66.77	7.23	Solidified stainless steel

TiB_2 platelets with thickness less than 1 μm, is clearly observed in the intermediate layer, as shown in Fig. 5.

As discussed in early reports [17], taking ball milling into mechanically activated reactive blends results in a reduced ignition temperature (by over 200 ℃) and an increased combustion velocity. Moreover, the introduction of ultrahigh gravity field causes the full-liquid products to rapidly deposit in the clearance underneath the unreacted blends, resulting in the dramatically increased combustion velocity by enhancing the transfer in heat, mass, and momentum from the liquid products to the reactants [5]. Therefore, by combining mechanical activation with ultrahigh gravity field, the combustion mode has transferred thermal explosion from steady SHS. The excessive chemical energy of combustion reaction can be almost completely used to heat full-liquid products due to the high heat accumulation from thermal explosion. Therefore, the actual combustion temperature in high gravity field is close to the adiabatic temperature of chemical reaction. As a result, following the combustion reaction completion in the crucible, the superfluous reaction heat also makes the surface of the stainless steel underneath the liquid ceramic partially molten. Because of the complete dissolvability among B, C, Ti, Fe, Cr, and Ni elements in liquid, liquid TiB_2–TiC ceramic and the molten stainless steel happen to dissolve into each other, initiating the strong interdiffusion under the concentration-induced chemical potential. In this infiltration process, the atoms of Ti, B, and C in liquid ceramic diffuse toward the molten stainless steel surface, while the atoms of Fe, Cr, and Ni in the molten stainless steel diffuse toward the liquid ceramic. Subsequently, the diffusion-controlled concentration gradient of each element arises between the liquid ceramic and the molten stainless steel, followed by the nucleation and the growth of the phases out of the melt.

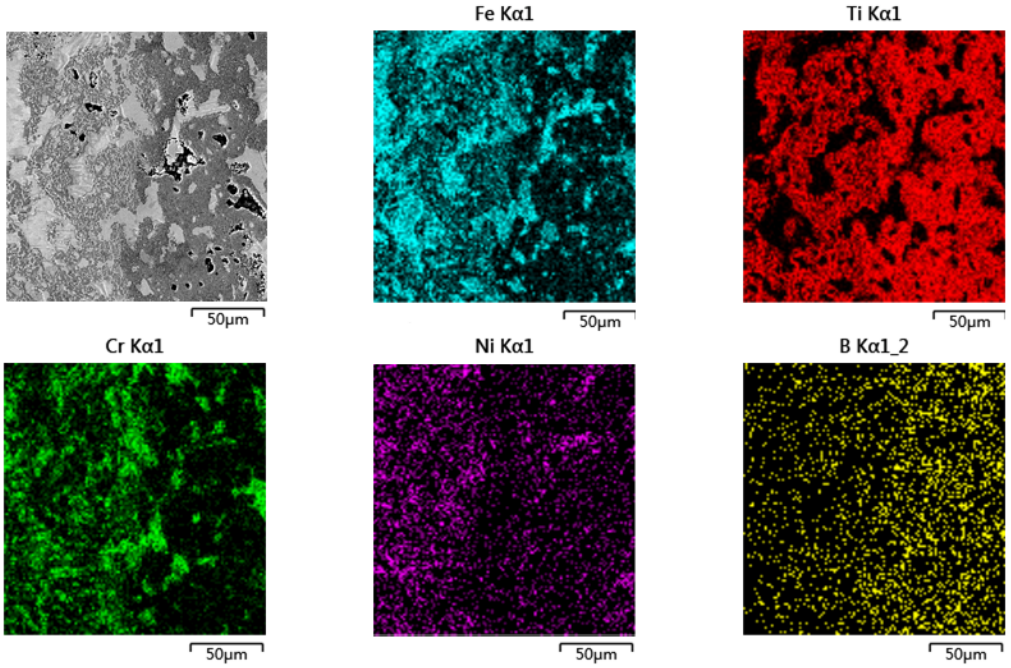

Fig. 6 EDS map scanning images of the joint area of the stainless steel and the ceramic.

In the experiment demonstrated above, the solidified TiB_2–TiC ceramic proves to be 66.7mol%TiB_2–TiC based on Eq. (1), which belongs to the hypereutectic group according to the binary equilibrium diagram of TiB_2–TiC system [3,4]. The TiB_2 is considered as the leading phase in nucleation process due to the higher concentration of B atoms than that of C atoms in liquid ceramic. Because crystal growth is usually associated with its melting entropy, and the crystal develops in facet growth mode if Jackson factor α ($=\Delta Sf/R$) is larger than 2 [18]. The melting entropy of TiB_2 and TiC is calculated to be 3.78 and 2.60, respectively. TiB_2 primary phases are considered to be more inclined to grow in the facet mode, thus the high degree of supercooling is required in the low-velocity growth of TiB_2 crystals. At the same time, TiB_2 has a hexagonal AlB_2-type structure of *P6*/*mmm* space group [18], and the hexagonal symmetry of TiB_2 enhances the anisotropy in crystallography. The high melting entropy of TiB_2 also enlarges the difference of different-index crystal planes in growth velocity, so TiB_2 primary phases ultimately develop the morphologies of the hexagonal platelets, which mostly seem to be small-bar grains due to the error of the detecting angle by FESEM, as shown in Fig. 3 and Fig. 5. In contrast, the face-centered structure of TiC strengthens the isotropy in crystallography, which makes it more inclined to develop the high-velocity non-facet growth in despite of its melting entropy larger than 2. Consequently, the TiB_2 platelets are hard to develop unlimitedly due to their high melting entropy and the enhanced anisotropic growth, in despite of the fact that TiB_2 platelets nucleate and grow as the primary phases. When it comes to the TiC secondary phases, because of a combination of their isotropic growth and high diffusion rate of C relative to B in metallic liquid, they grow rapidly once they begin to nucleate, and ceaselessly compete for growth space and free Ti atoms against TiB_2 primary phases. In this case, some fine TiB_2 platelets are surrounded by TiC irregular grains and stop to grow, thereby presenting the unique solidified microstructure where a number of fine TiB_2 platelets are embedded in irregular TiC grains, as showed in Fig. 3 and Fig. 5. Moreover, the dissolution of the molten stainless steel into the liquid ceramic occupies the growth space of TiB_2 primary phases mostly, and makes TiB_2 crystals more difficult to grow. Therefore, ultrafine-grained microstructures characterized by the thickness of TiB_2 primary phases smaller than 1 μm develop in either the intermediate or the nearby ceramic, as shown in Fig. 5. In addition, C atom diffuses into the molten stainless steel more widely than B atom does, just because of the high diffusion rate of C relative to B in ceramic liquid, thereby presenting the wider graded distribution of (Fe, Cr, Ni) enriched TiC_{1-x} phases than that of the others in the intermediate, as shown in Fig. 7 and Fig. 8. And the EDS results in Table 2 also certify this result

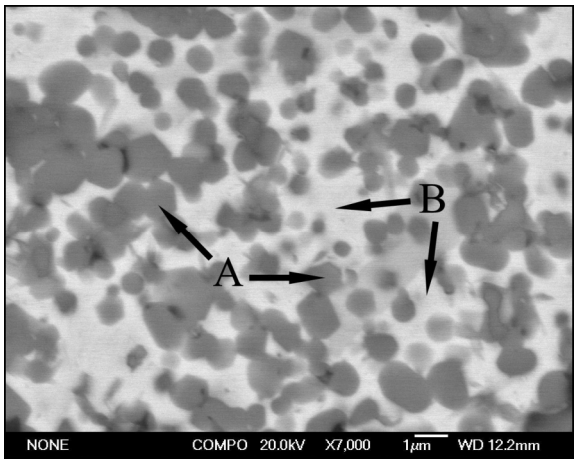

Fig. 7 (Fe, Cr, Ni) enriched TiC_{1-x} carbides distributed at solidified stainless steel.

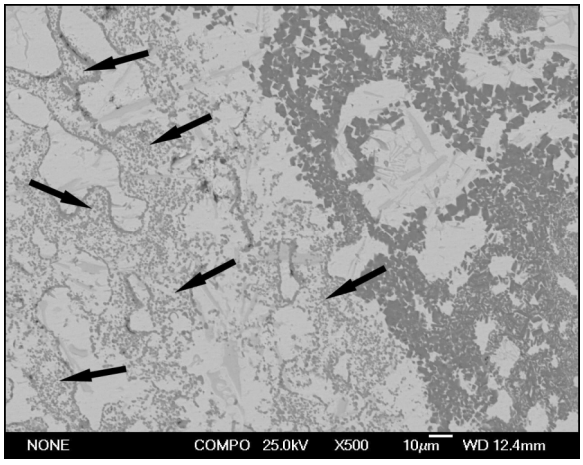

Fig. 8 Distribution of (Fe, Cr, Ni) enriched TiC_{1-x} carbides from the intermediate to solidified stainless steel surface.

Table 2 Composition of the solidified stainless steel surface in Fig. 7 (unit: at%)

Position	Ti	C	Cr	Fe	Ni	Determined phase
A	44.86	33.51	6.82	7.80	7.01	(Fe, Cr, Ni) enriched TiC_{1-x}
B	6.01	—	18.35	68.78	6.86	Solidified stainless steel

mentioned above.

At the final stage of solidification, due to the dissolution of the molten stainless steel into the ceramic liquid, the residual liquid consisting mainly of the molten stainless steel spreads out at the surfaces of TiB_2 and TiC solids, and infiltrates the shrinkage cavities between the ceramic solids under a combination of capillary action and ultrahigh gravity field. So the densification of the intermediate layer and the ceramic is promoted. Subsequently, the molten stainless steel happens to aggregate and develop the coarse metallic alloy in the intermediate, or solidify to form the boundaries of TiB_2 and TiC solids (as shown in Fig. 9), thereby presenting in the intermediate layer with the hybrid microstructures, as it reveals that different-size and different-morphology Fe–Cr–Ni alloy phases alternate with TiB_2 platelets and irregular TiC grains.

In conclusion, the formation mechanism of the laminated composite materials of TiB_2–TiC/1Cr18Ni9Ti fabricated by combustion synthesis in ultrahigh gravity field involves three stages: the formation of thermal explosion caused by a combination of mechanical activation and ultrahigh gravity field to yield high-temperature TiB_2–TiC ceramic liquid during the first stage; the formation of the molten stainless steel to dissolve TiB_2–TiC liquid, thereby yielding the diffusion-controlled concentration gradient from the ceramic liquid to the alloy liquid during the second stage; and the formation of rapid sequent solidification of the ceramic and the alloy during the third stage (as shown in Fig. 10). Therefore, the laminated composite materials are achieved in continuously graded composition and microstructure from the ceramic to the stainless steel. And, between

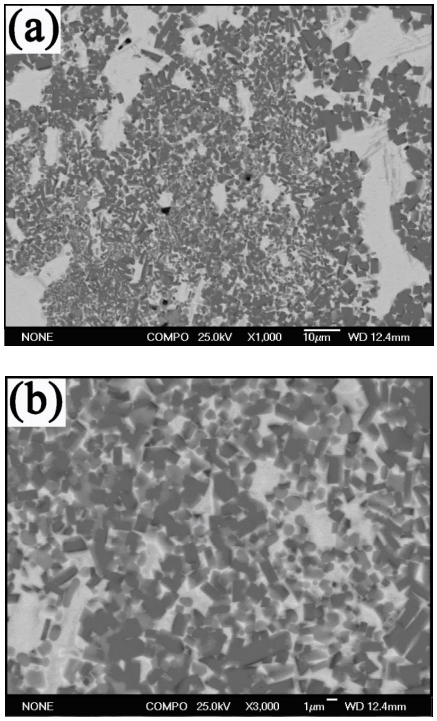

Fig. 9 Hybrid microstructure in the intermediate layer: (a) the segregation of the alloy phases; (b) the alloy phases distributed in the inter-region of TiB_2 and TiC.

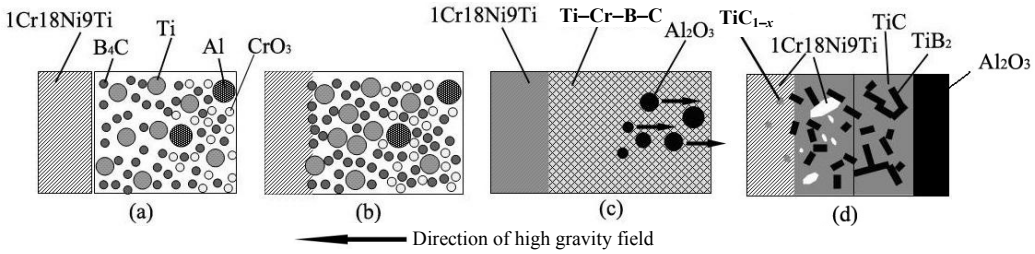

Fig. 10 Formation of the TiB_2–TiC/1Cr18Ni9Ti laminated composite by combustion synthesis in ultrahigh gravity field.

the ceramic and the alloy, the hybrid microstructure of multilevel and scale-span is presented with different-size, different-morphology Fe–Cr alloy phases alternating with TiB_2 platelets and irregular TiC grains in size from micrometer to nanometer.

Figure 11 shows the FESEM image of shear fracture surface of the ceramic/metal joint, and the shear strength of ceramic/metal joint was measured as 320 MPa. The experiments reveals that the shear fracture always takes place in the intermediate area near the stainless steel substrate where Al_2O_3 inclusions and cavities become the weak points and the crack sources in stress concentration. Hence, it can obtain higher joint strength by removing Al_2O_3 inclusions and cavities in combustion synthesis, so the higher high gravity field and the enough combusiton heat are necessary in these experiments.

4 Conclusions

By applying combustion synthesis in ultrahigh gravity field to prepare solidified TiB_2–TiC ceramic, the laminated composite materials of TiB_2–TiC ceramic to 1Cr18Ni9Ti stainless steel are achieved in continuously graded microstructure via liquid dissolution and atomic interdiffusion. XRD, FESEM, and EDS results show that the ceramic is composed of a number of fine TiB_2 platelets, irregular TiC grains, and a few of Cr metallic binder. And the physical and mechanical properties reveal that the density, hardness, and fracture toughness of the ceramic are 4.3 g/cm^3, 18±1.5 GPa, and 13.5±1.8 MPa·m$^{1/2}$, respectively. The blend of TiB_2–TiC ceramic to stainless steel consists of three-layer structures, i.e., the TiB_2–TiC ceramic layer, the intermediate layer, and the stainless steel substrate. The key formation principle of the laminated composite materials of TiB_2-based ceramic to stainless steel by combustion synthesis in ultrahigh gravity field is considered to the following three elements: the formation of high-temperature TiB_2–TiC ceramic liquid during thermal explosion; the separation of Al_2O_3 drops and bubbles from ceramic liquid under high gravity field; the interdiffusion and filling between the ceramic liquid and the fused stainless steel surface. As a result, the laminated composite materials of TiB_2–TiC/1Cr18Ni9Ti are achieved in multilevel, scale-span hybrid microstructure, and the shear strength of ceramic/metal joint is measured as 320 MPa.

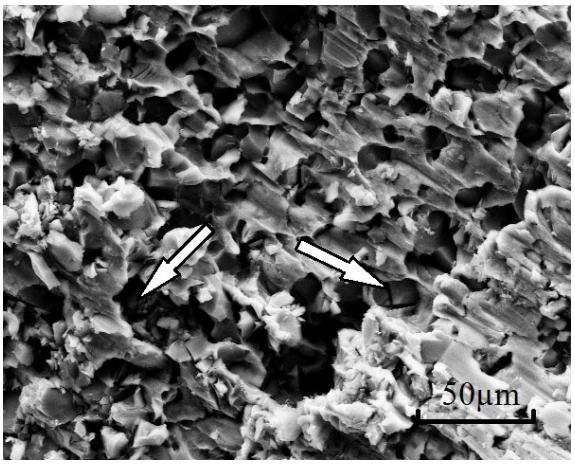

Fig. 11 FESEM image of shear fracture surface of the ceramic/metal joint.

Acknowledgements

This work is sponsored by the National Natural Science Foundation of China (Grant No. 51072229).

References

[1] Zhang GJ, Jin ZZ, Yue XM. Effects of Ni addition on

mechanical properties of TiB_2/SiC composites prepared by reactive hot pressing (RHP). *J Mater Sci* 1997, **32**: 2093–2097.

[2] Lee TW, Lee CH. Microstructure and mechanical properties of TiB_2/TiAl composites produced by reactive sintering using a powder extrusion technique. *J Mater Sci Lett* 1999, **18**: 801–803.

[3] Vallauri D, Adrián ICA, Chrysanthou A. TiC–TiB_2 composites: A review of phase relationships, processing and properties. *J Eur Ceram Soc* 2008, **28**: 1697–1713.

[4] Degrave IE, Udalov YP. Composite powders of the TiC–TiB_2 system. *Glass Ceram* 2000, **57**: 396–398.

[5] Huang X, Zhang L, Zhao Z, *et al.* Microstructure transformation and mechanical properties of TiC–TiB_2 prepared by combustion synthesis in high gravity field. *Mat Sci Eng A* 2012, **553**: 105–111.

[6] Zhang Y, Feng D, He Z, *et al.* Progress in joining ceramics to metals. *J Iron Steel Res Int* 2006, **13**: 1–5.

[7] Huang X, Zhao Z, Zhang L. Layered composite of TiC–TiB_2 to Ti–6Al–4V in graded composition by combustion synthesis in high-gravity field. *J Phys*: *Conf Ser* 2013, **419**: 012027.

[8] Yin C, Chen YQ, Zhong SM, *et al*. Fractional-order sliding mode based extremum seeking control of a class of nonlinear system. *Automatica* 2014, **50**: 3173–3181.

[9] Yin C, Stark B, Chen YQ, *et al.* Adaptive minimum energy cognitive lighting control: Integer order vs fractional order strategies in sliding mode based extremum seeking. *Mechatronics* 2013, **23**: 863–872.

[10] Bever MB, Duwez PE. Gradients in composite materials. *Mater Sci Eng* 1972, **10**: 1–8.

[11] Huang X, Zhao Z, Zhang L, *et al.* The effects of ultra-high-gravity field on phase transformation and microstructure evolution of the TiC–TiB_2 ceramic fabricated by combustion synthesis. *Int J Refract Met H* 2014, **43**: 1–6.

[12] Morsi K. The diversity of combustion synthesis processing: A review. *J Mater Sci* 2012, **47**: 68–92.

[13] Chaudhari YA, Mahajan CM, Jagtap PP, *et al.* Structural, magnetic and dielectric properties of nano-crystalline Ni-doped $BiFeO_3$ ceramics formulated by self-propagating high-temperature synthesis. *J Adv Ceram* 2013, **2**: 135–140.

[14] Contreras L, Turrillas X, Vaughan GBM, *et al.* Time-resolved XRD study of TiC–TiB_2 composites obtained by SHS. *Acta Mater* 2004, **52**: 4783–4790.

[15] Mahmoodian R, Hassan MA, Hamdi M, *et al. In situ* TiC–Fe-Al_2O_3–TiAl/Ti_3Al composite coating processing using centrifugal assisted combustion synthesis. *Composites Part B* 2014, **59**: 279–284.

[16] Huang X, Zhao Z, Zhang L. Fusion bonding of solidified TiC–TiB_2 ceramic to Ti–6Al–4V alloy achieved by combustion synthesis in high-gravity field. *Mat Sci Eng A* 2013, **564**: 400–407.

[17] Aminikia B. Investigation of the pre-milling effect on synthesis of nanocrystalline TiB_2–TiC composite prepared by SHS method. *Powder Technol* 2012, **232**: 78–86.

[18] Kurz W, Fisher DJ. *Fundamentals of Solidification*, 4th edn. Switzerland: Trans Tech Publications Ltd, 1998.